Near-barrier transfer reactions in the $^{36}S+^{144,154}Sm$ systems

J. O. Fernández Niello,* J. E. Testoni, M. di Tada, and A. J. Pacheco
TANDAR, Departamento de Física, Comisión Nacional de Energía Atómica, Avenida del Libertador 8250, 1429 Buenos Aires, Argentina

D. R. Napoli,† A. M. Stefanini, L. Corradi, B. Million,‡ M. Narayanasamy,§ and P. Spolaore
Istituto Nazionale di Fisica Nucleare, Laboratori Nazionali di Legnaro, Padova, Italy

S. Beghini, G. Montagnoli, F. Scarlassara, G. F. Segato, C. Signorini, and F. Soramel
Dipartimento di Fisica, Università e Istituto Nazionale di Fisica Nucleare, Padova, Italy
(Received 11 April 1991)

Angular distributions and Q-value spectra for transfer reactions in the systems $^{36}S+^{144,154}Sm$ have been measured at two energies close to the Coulomb barrier. Mass and charge identification was achieved using a time-of-flight system followed by an ionization chamber. Transfer probabilities were analyzed considering direct and sequential barrier penetration mechanisms. The dependence of the cross sections on the static quadrupole deformation of the targets was compared with the predictions of a semiclassical approach. The relative yields of the different channels were analyzed in the light of a random-walk approach based on the reaction Q values.

PACS number(s): 25.70.−z

I. INTRODUCTION

During the last few years, much experimental and theoretical effort has been devoted to the study of heavy-ion reactions at bombarding energies near the Coulomb barrier. Attention has been focused on these types of processes as a result of the observed enhancement of fusion cross sections compared to one-dimensional models for a variety of systems. Among other aspects (such as deformation of the participant ions, neck formation, coupling to inelastic channels), the importance of transfer channels in producing such an enhancement has been predicted [1–3]. The mechanism of heavy-ion transfer reactions may be affected by collective features as well as by single-particle effects. On the other hand, experimental data suggest a correlation between transfer cross sections and the static deformation of one of the reaction partners [4,5]. On the other hand, the reaction mechanism is also influenced by nuclear structure effects reflecting the single-particle states populated in the process.

Static nuclear deformation effects in transfer probabilities may be investigated in reactions using targets of the same element whose isotopes have different shapes. The isotopes of samarium are an excellent choice in this approach as they exhibit a wide range of deformation, from the spherical, semimagic, ^{144}Sm to the well-deformed ^{154}Sm. Prior to this work, near-barrier transfer on these targets was studied using the doubly magic projectile ^{16}O [4]. Larger cross sections for the ^{154}Sm case were observed which reflect the effect of target deformation [5].

In this work we have studied transfer reactions in the $^{36}S+^{144,154}Sm$ systems at two energies around the Coulomb barrier. This neutron-magic sulfur isotope is an appropriate projectile for isolating the deformation effects of the targets since it is almost spherical. It was our aim to address the question of whether the effects of deformation, observed in the reactions induced by ^{16}O, are still dominant or if other structure effects show up with ^{36}S projectiles. Another aspect that may be investigated is the possible influence of the mass-asymmetry degree of freedom on transfer reactions when using a heavier, but still spherical, projectile.

The experimental setup is described in Sec. II, and the analysis of the experimental data is detailed in Sec. III. Section IV contains semiclassical calculations of transfer probabilities, an analysis of the effects of nuclear static deformations, and a study of transfer cross sections in terms of Q-value considerations. A summary is given in Sec. V.

II. EXPERIMENTAL METHOD

The experiment was carried out at the XTU tandem accelerator of the Laboratori Nazionali di Legnaro. The analysis and reduction of the data were done at the TANDAR Laboratory in Buenos Aires. The measurements were performed at two bombarding energies (142 and 155 MeV) in the vicinity of the Coulomb barriers [6],

*On leave at Sektion Physik, Universität München, 8046 Garching, Germany.
†On leave from TANDAR, Buenos Aires, Argentina.
§On leave from Nuclear Science Centre, JNU Old Campus, New Delhi, India.
‡Present address: INFN–Sezione di Milano, Italy.

which are 143.2 and 139.8 MeV for the $^{36}S+^{144}Sm$ and $^{36}S+^{154}Sm$ reactions, respectively. The ^{36}S beams were produced from a sputter source with Ag_2S cone enriched to about 40% in mass 36 and had typical intensities ranging from 5 to 20 particle nA. The ^{144}Sm and ^{154}Sm targets were enriched to 96.5% and 98.7%, respectively. They had an approximate thickness of 100 $\mu g/cm^2$ and were evaporated onto 30 $\mu g/cm^2$ carbon backings.

The experimental setup consisted of a sliding-seal scattering chamber followed by two microchannel plate detectors (MCP's) and an ionization chamber (IC) with subdivided anode in order to obtain $E-\Delta E$ information. The IC was filled with CH_4 at pressures ranging from 120 to 150 torr and had an entrance window made of stretched polypropilene about 50 $\mu g/cm^2$ thick. Details on the IC are given elsewhere [7]. Two different flight paths were used by setting the MCP's at distances of 144 and 233 cm between each other; the corresponding solid angles of the setup were 0.51 and 0.31 msr, respectively. The transmission of the detection system, considering the MCP's and the entrance grid of the IC, was about 74%. Moreover, the coincidence efficiency was measured to be about 95%. Two monitor detectors mounted at $\theta_{lab}=\pm 16°$ served to establish absolute normalizations.

Angular distributions were measured in the range $75° < \theta_{lab} < 120°$ at $E_{lab}=155$ MeV and $105° < \theta_{lab} < 135°$ at $E_{lab}=142$ MeV. The choice of the angular range for the run at 155 MeV was based on the predicted grazing angles [6] for the different systems ($\theta_{graz}=105°$ and 98° for ^{144}Sm and ^{154}Sm, respectively). At the lowest bombarding energy, the limit $\theta_{lab}=135°$ was given by mechanical restrictions of the sliding-seal chamber. The determination of the total energy, considering kinetic-energy spread, straggling in the IC window and target thickness, had uncertainties of about 1.5%.

III. DATA ANALYSIS AND EXPERIMENTAL RESULTS

Particle identification was achieved by measuring the total energy of the ejectiles (E_T), their energy loss in a differential zone of the gas detector (ΔE), and the time of flight (TOF) between the MCP's. The ΔE resolution of the IC signals allowed a precise determination of the yields of the different charged-particle transfer channels. As an example, Fig. 1 shows the identification of the different elements obtained from the E_T-ΔE plot for the reactions $^{36}S+^{144}Sm$ and $^{36}S+^{154}Sm$ taken at $E_{lab}=155$ MeV and $\theta_{lab}=85°$. These scatter plots clearly exhibit differences between the two systems. On the one hand, reactions on the ^{154}Sm target present essentially charge stripping events that correspond to ejectiles with $Z=14$ and 15. In addition to these channels, charge pickup events leading to Cl and Ar are observed in the case of ^{144}Sm.

Mass spectra for each Z were obtained by linearization of E_T-TOF plots and subsequent projection onto the mass axis. A mass resolution $\Delta A/A \approx 1/50$ full width at half maximum (FWHM) was typically obtained. The identification of the different masses was helped by summing up the mass spectra over the different angles. The

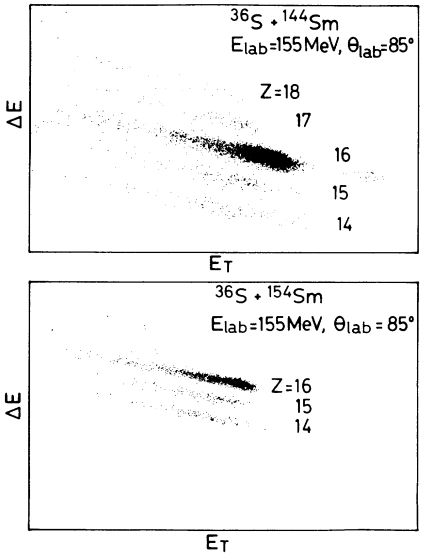

FIG. 1. Scatter plots E_T-ΔE obtained for the reaction $^{36}S+^{144}Sm$ and $^{36}S+^{154}Sm$ at $E_{lab}=155$ MeV and $\theta_{lab}=85°$.

centroids and widths of the peaks appearing in these summed spectra were used as an additional test for the identification of ejectile masses in the spectra for each angle.

Angular distributions of the different ejectiles for both systems are shown in Figs. 2 and 3 for ^{144}Sm and ^{154}Sm, respectively, at both beam energies. The errors bars take into account statistical fluctuations as well as uncertainties in mass identification and background determination. The angular distributions for the bombarding energy slightly above the barrier (155 MeV) show bell-like shapes, 20°–30° wide, centered between $\theta_{c.m.}=100°$ and 110° for ^{144}Sm and between $\theta_{c.m.}=95°$ and 100° for ^{154}Sm. Maximum values of the differential cross sections range, for the analyzed reactions, from 2.5 to 10 mb/sr for the $^{36}S+^{144}Sm$ system and from 8 to 25 mb for the $^{36}S+^{154}Sm$ system.

Differential cross sections at $E_{lab}=142$ MeV were measured in the range $\theta_{c.m.}=117°-145°$. This bombarding energy corresponds to 0.99 of the Coulomb barrier for the $^{36}S+^{144}Sm$ system and 1.02 of the barrier for the $^{36}S+^{154}Sm$ case. Ratios between maxima of the differential cross sections at 155 and 142 MeV seem to be generally greater for the ^{144}Sm than for the ^{154}Sm case.

Figure 4 summarizes the transfer cross sections for ^{144}Sm [Fig. 4(a)] and ^{154}Sm [Fig. 4(b)] at the two bombarding energies, showing values for the dominant exit channels which our experimental setup was able to resolve in mass. These cross sections were obtained by numerical integration of a smooth curve interpolating the experimental points for each angular distribution (see Figs. 2 and 3). The shadowed regions indicate some evidence for the corresponding transfer channels at both energies. In each case an upper limit of about 25% of the charged-particle transfer cross section for the relevant Z

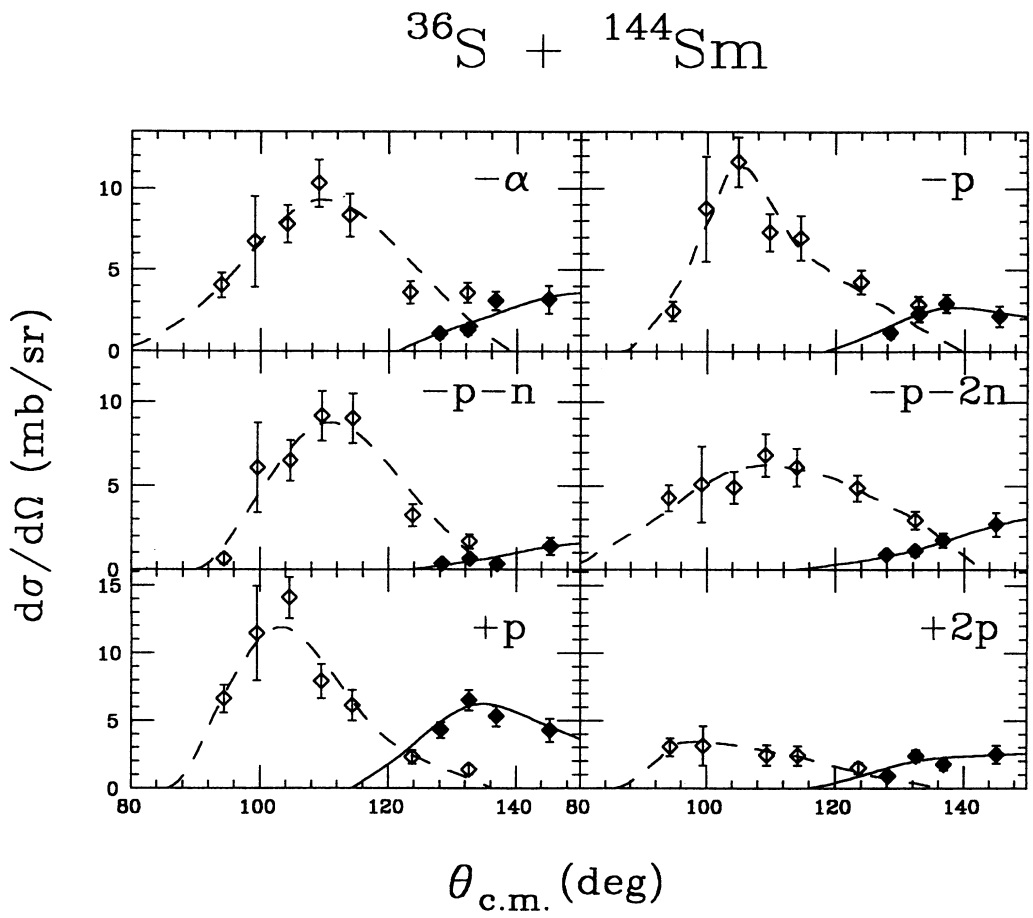

FIG. 2. Angular distributions for different transfer channels for $^{36}S+^{144}Sm$ at $E_{lab}=155$ MeV (open symbols) and 142 MeV (solid symbols). The lines correspond to the interpolation used in the determination of the total transfer cross sections. Plus and minus signs indicate pickup and stripping reactions, respectively.

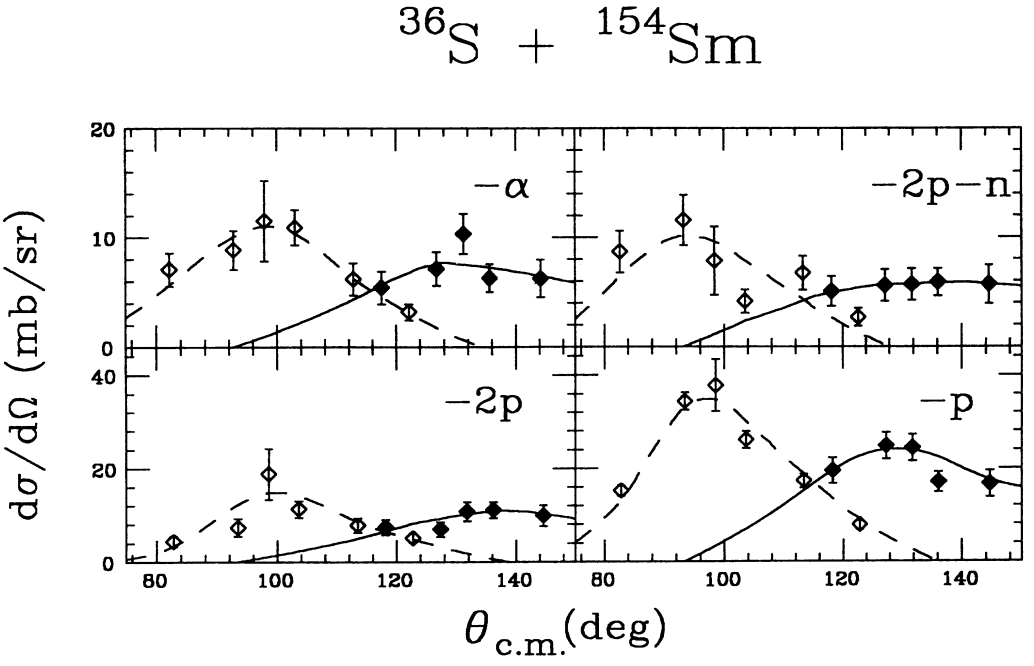

FIG. 3. Same as Fig. 2 for the ^{154}Sm target.

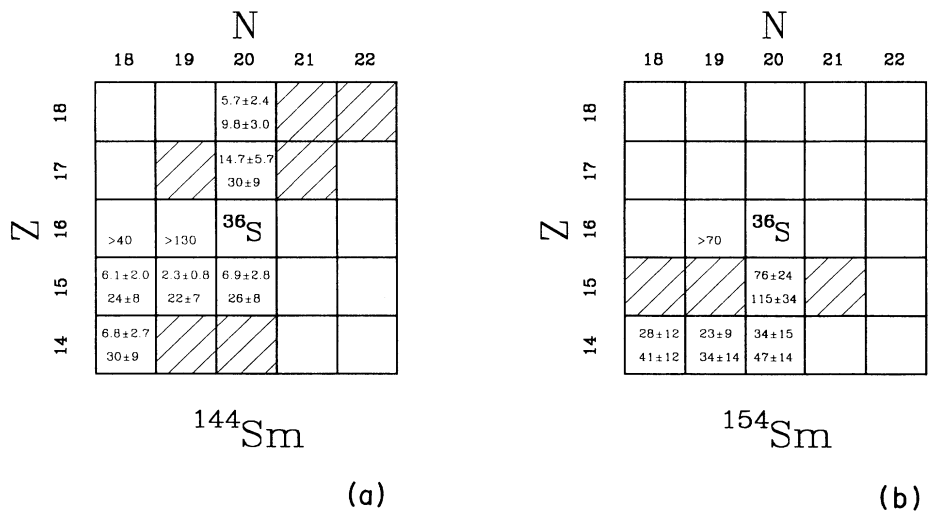

FIG. 4. Transfer cross sections for the (a) $^{36}S+^{144}Sm$ and (b) $^{36}S+^{154}Sm$ systems at $E_{lab}=142$ MeV (upper values) and 155 MeV (lower values). The shadowed regions indicate some evidence of transfer (see text).

was estimated. These charged-particle transfers cross sections σ_{tr}, which were obtained by integration of the differential cross sections extracted from the E-ΔE scatter plots, are given in Table I. As can be seen in Fig. 4, silicon ejectiles with $A=34$, 33, and 32 ($2p$, $2p$-$1n$, and α-particle stripping, respectively) are present with similar intensities for ^{154}Sm, while for ^{144}Sm the ^{32}Si isotope (i.e., α-particle stripping) dominates. This feature is reversed in the case of phosphorus ejectiles. The ^{154}Sm target shows a dominant peak in $A=35$ ($1p$ stripping), while for

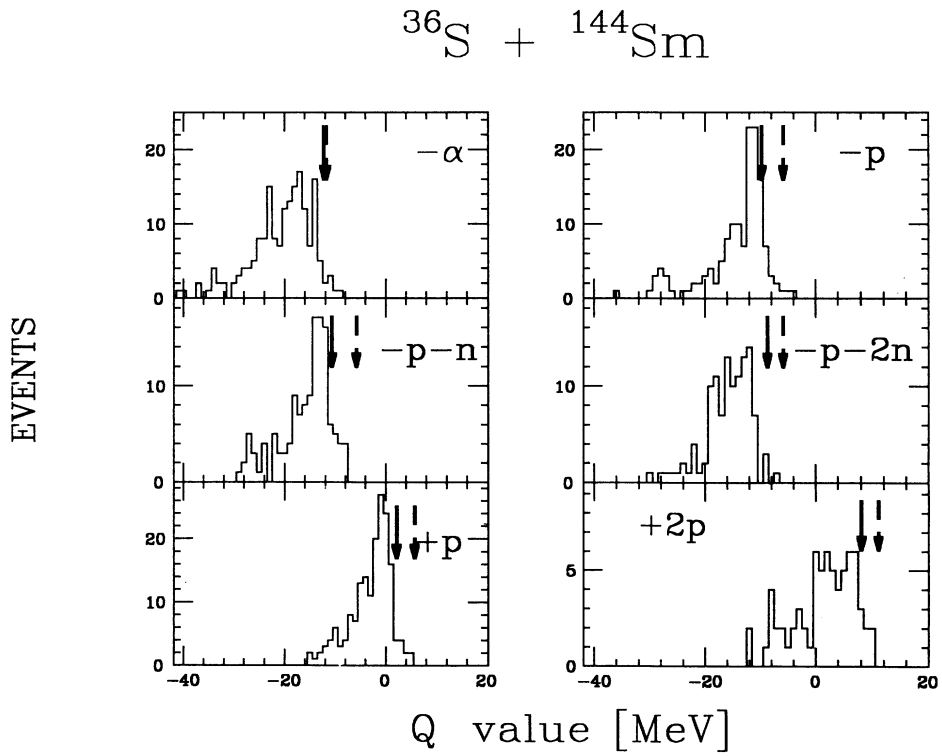

FIG. 5. Q-value spectra for different transfer channels in the $^{36}S+^{144}Sm$ reaction at $E_{lab}=155$ MeV. Solid (dashed) vertical arrows indicate the position of the ground-state (optimum) Q values. Plus and minus signs indicate pickup and stripping reactions, respectively.

TABLE I. Charge-transfer cross sections.

Z ejectile	$\sigma_{tr}(E_{lab}=142$ MeV) (mb) $^{36}S+^{144}Sm$	$^{36}S+^{154}Sm$	$\sigma_{tr}(E_{lab}=155$ MeV) (mb) $^{36}S+^{144}Sm$	$^{36}S+^{154}Sm$
14	17.6±2.8	96.4±6.7	68.4±6.7	159.8±14.8
15	20.4±3.0	119.7±13.1	87.8±8.2	213.4±21.6
17	22.7±3.5		52.2±5.7	
18	8.0±1.8		22.4±2.2	

the ^{144}Sm target the strengths are evenly distributed among $A=35$, 34, and 33 ($1p$, $1p$-$1n$, and $1p$-$2n$ stripping, respectively).

As mentioned above, charge pickup reactions are significant only for $^{36}S+^{144}Sm$; charge $Z=17$ is mainly associated with $A=37$ ($1p$ pickup) and charge $Z=18$ with $A=38$ ($2p$ pickup).

The case of pure neutron transfer posed special difficulties because of the mass resolution, the tails coming from the dominant elastic peak, and the limited statistics in some cases. Therefore, we were not able to uniquely identify these transfer events. Neutron stripping seems to be more important than neutron pickup. In some cases lower limits for the cross sections could be established (See Fig. 4). For the ^{154}Sm target, pure neutron transfer is also evident, but not so significant.

The mass and charge identification allows the determination of the Q-value distributions for the various exit channels. Q-value spectra taken at $E_{lab}=155$ MeV for the $^{36}S+^{144}Sm$ and $^{36}S+^{154}Sm$ reactions are shown in Figs. 5 and 6, respectively. To obtain these spectra all runs of the angular distributions were summed up. Generally, Q-value distributions begin at the ground-state Q value. The α-particle stripping in the case of the $^{36}S+^{154}Sm$ system seems to be the exception since the Q-value peak is shifted by almost 10 MeV (a hint of a similar behavior is seen in the $2p$-n and $2p$ stripping Q-value distributions). The centroids of the distributions are in reasonable agreement with calculated optimum Q values, with the obvious exception of those cases where the latter are not negative enough compared to the corresponding ground state Q values. Excitation energies extend over a range of 15–20 MeV.

IV. DISCUSSION

A. Semiclassical description of transfer probabilities

Differential transfer cross sections as a function of center-of-mass angles are commonly presented as transfer probabilities versus distances of closest approach. Experimental transfer probabilities are readily obtained as the ratio between the cross section at a given angle for the relevant transfer channel and the sum of the cross sections for all the processes (including elastic and inelastic scattering) contributing to the emission of projectilelike fragments at that same angle:

$$P_x(\theta)=\frac{d\sigma_x(\theta)/d\Omega}{\sum_y [d\sigma_y(\theta)/d\Omega]} . \quad (1)$$

Assuming Coulomb trajectories, the distance of closest

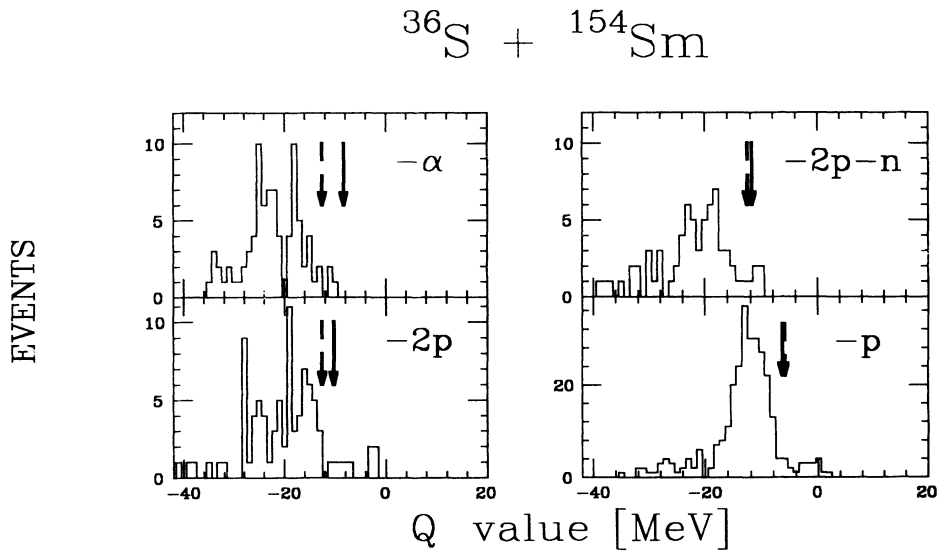

FIG. 6. Same as Fig. 5 for the ^{154}Sm target.

approach, D, is calculated as a function of the scattering angle by

$$D=\frac{Z_1Z_2e^2}{2E_{\rm cm}}\left[1+\frac{1}{\sin(\theta_{\rm cm}/2)}\right] . \quad (2)$$

This presentation was early recognized as particularly useful in the study of neutron transfer reactions occurring at relatively large internuclear distances compared to the range of nuclear forces. In this regime the transfer process is expected to be well described by semiclassical formalisms. As a further approximation [8], only the minimum internuclear distance is considered for the determination of the transfer probability. This probability is governed by the tunneling of an effective barrier related to the binding energies of the neutron in the donor and acceptor cores. According to this description, the dependence of the transfer probability P_x as a function of D follows a characteristic exponential law:

$$P_x \propto \exp(-\alpha D) . \quad (3)$$

The normalization constant can be factorized into two contributions, one containing a Q-value dependence, whereas the other is essentially given by the corresponding spectroscopic factor [8]. The exponential decay constant can be written as

$$\alpha=(2\mu B_{\rm eff}/\hbar^2)^{1/2} , \quad (4)$$

where μ is the reduced mass and $B_{\rm eff}$ is an effective binding energy. This exponential behavior has been experimentally verified for a variety of systems (see, e.g., Ref. [8]), although the observed values of the decay constants do not always agree with simple expectations from the model.

Figures 7 and 8 show transfer probabilities P_x versus the reduced distance of closest approach, $d_0=D/(A_T^{1/3}+A_P^{1/3})$, corresponding to the ^{36}S+^{144}Sm and ^{36}S+^{154}Sm systems, respectively, for the various transfer channels measured in the present work. Data for the two bombarding energies were included in each case. A general feature exhibited by all these plots is, within experimental errors, an exponential decay at large distances, suggesting tunneling processes. The comparison between the two bombarding energies shows a systematic difference consisting of a slower decay for 155 MeV than for 142 MeV. This difference is in principle inconsistent with the simple idea of the transfer being determined only by the minimum internuclear distance given by Eq. (2). A similar energy dependence has also been observed for one- and two-neutron transfer reactions in ^{28}Si+^{208}Pb [9] and, to some extent, in proton as well as neutron transfer in ^{50}Ti+^{90}Zr [8]. This energy dependence of the transfer probabilities has been tentatively attributed to shortcomings in the evaluation of the deflection function implied by Eq. (2), which neglects the nuclear contribution to the trajectories, although this effect is expected to be less important as the apsidal distance increases. Another possible explanation relates to the total Q value (i.e., including the excitation energies) of the reaction. If the latter does

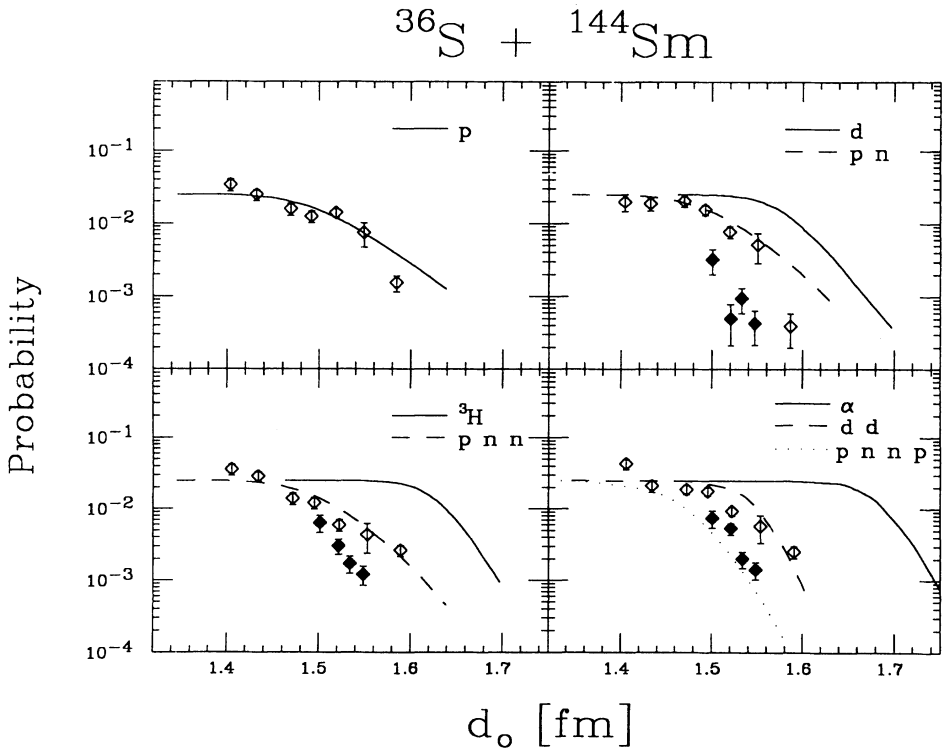

FIG. 7. Transfer probabilities for the ^{36}S+^{144}Sm reaction plotted vs the reduced distance of closest approach. Predictions based on direct and sequential tunneling are shown. Open symbols corespond to $E_{\rm lab}=155$ MeV and solid symbols to $E_{\rm lab}=142$ MeV.

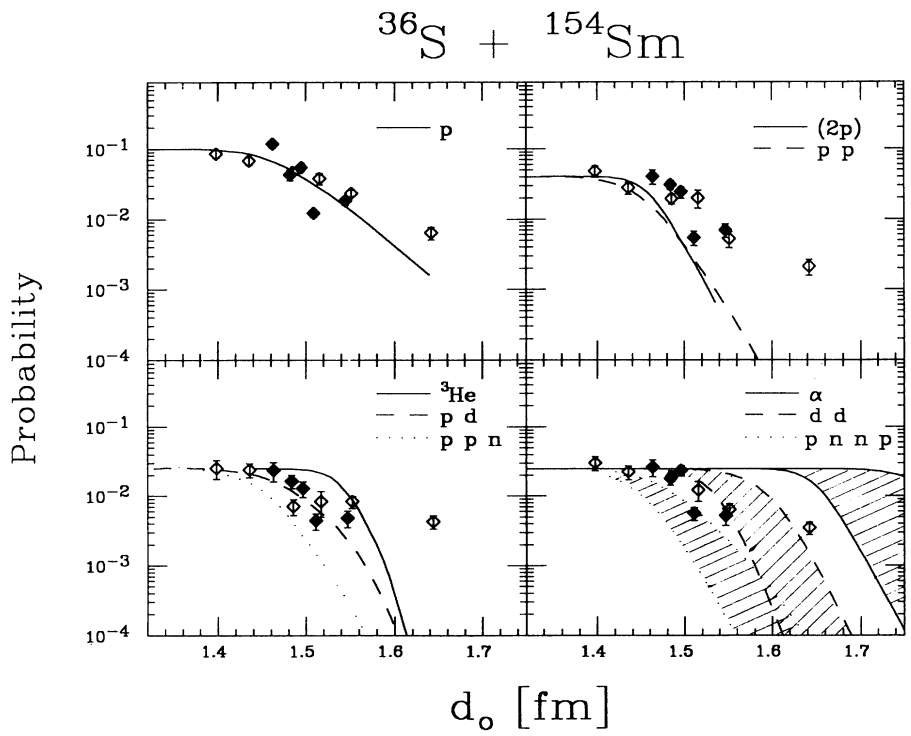

FIG. 8. Same as Fig. 7 for the ^{154}Sm target. The shaded bands correspond to different possible sequences for the occurrence of excitation and transfer at each step (see text).

not agree with the kinematical selectivity rule that is simply based on the requirement of a smooth matching of trajectories in the entrance and exit channels [6],

$$Q_{\text{opt}}=E_{\text{cm}}\left[\frac{Z_i^f Z_p^f}{Z_i^i Z_p^i}-1\right], \tag{5}$$

then a deviation from Eq. (2) would be predicted even for pure Coulomb trajectories before and after transfer at the distance of closest approach. Unfortunately, the present data do not allow us to evaluate this assumption because only the results at 155 MeV could be adequately processed because of poor statistics at the lowest bombarding energy.

In order to achieve a somewhat more qualitative understanding of the present data, we performed calculations based on the simple model of Brosa and Gross [10]. These authors consider that the transferred particle (a proton or a neutron) moves under the influence of the combined potentials created by the donor and acceptor cores:

$$U_{p(n)}(D,r)=U_{p(n),1}(r)+U_{p(n),2}(D-r), \tag{6}$$

where D is the distance between the cores 1 and 2, p (n) means proton (neutron), and r indicates the spatial coordinate of the transferred particle with respect to the donor core. In the case of a proton, the potential created by the donor core may be decomposed into nuclear and Coulomb contributions:

$$U_{p,1}(r)=V_{p,1}^0(r)\{1+\exp[(r-R_1)/a\}^{-1}+V_{\text{Coul},1}(r), \tag{7}$$

where R_1 and a are the core radius and diffuseness, respectively, and

$$V_{\text{Coul},1}(r)=\begin{cases}\dfrac{e^2Z_1}{r}, & r_1\geq R_{c_1}\\ e^2Z_1\left[\dfrac{3}{2R_{c_1}}-\dfrac{r^2}{2R_{c_1}^3}\right], & r_1<R_{c_1},\end{cases} \tag{8}$$

R_{c_1} being the Coulomb radius. In the case of a neutron,

$$U_{n,1}(r)=V_{n,1}^0(r)\{1+\exp[(r-R_1)/a]\}^{-1}. \tag{9}$$

Expressions similar to Eqs. (7)–(9) hold for the acceptor core (core 2) if the coordinate r is replaced by $D-r$.

Finally, the model assumes that the potential barrier relevant to the transfer process can be approximated by an inverted parabola, thus allowing the use of the analytic expression of Hill and Wheeler [11] for the transmission probabilities P:

$$P=\left[1+\exp\left[\frac{2\pi}{\hbar\omega}(V+S)\right]\right]^{-1}, \tag{10}$$

where V is the energy corresponding to the top of the barrier, S is the separation energy of the transferred particle in the core, and ω is related to the barrier width through the expression

$$\omega=\left[\frac{1}{\mu}\frac{\partial^2 U}{\partial r^2}\right]^{1/2}. \tag{11}$$

For the calculations performed in the present analysis, we have taken from Ref. [10] the following values for the parameters of Eqs. (7) and (8):

$$V^0 = \left[-51 \pm 33 \frac{N-Z}{A} \right] \text{ MeV} \quad (12)$$

(+ for neutrons and − for protons; N, Z, and A refer to the core),

$$R = 1.27 A^{1/3} \text{ fm} ,$$

$$a = 0.67 \text{ fm} ,$$

$$R_c = 1.2 A^{1/3} \text{ fm} .$$

As an example, Fig. 9 shows the potential corresponding to the case of one-proton stripping in $^{36}S + ^{144}Sm$ (i.e. the potential created by the ^{35}P and ^{144}Sm cores) at an internuclear distance of 13 fm. The dashed curve illustrates the quality of the parabolic fit to the barrier. The zero-energy level has been arbitrarily taken as that corresponding to the three fragments (two cores plus the transferred proton) separated by infinite distances. The energy levels indicated in both wells correspond to the binding energies E_b of the proton in ^{36}S and ^{145}Eu.

In order to analyze our experimental results, we have extended the applicability of an expression similar to Eq. (6) to the case of the direct transfer of a complex fragment by simply adding the contributions from the individual nucleons to the potential. Therefore, the parameter V_x^0, corresponding to a complex fragment x formed by z protons and n neutrons, is taken as

$$V_x^0 = z V_p^0 + n V_n^0 . \quad (13)$$

In a similar way the Coulomb potential is given by multiplying Eq. (8) and the equivalent equation for the acceptor core by z. A more accurate procedure for the calculation of V_x^0 would require fits to the experimental binding energies, but we will postpone the discussion on the validity of the assumption given by Eq. (13). For each transfer the energy level used in the evaluation of $V+S$ [see Fig. 9 and Eq. (10)] was taken as that corresponding to the least-bound case if we compare separation energies in both cores, so as to ensure the availability of states at both sides of the barrier. This choice of energy levels contains the implicit assumption that the excitation process that accounts for the experimental Q values occurs as a second step following barrier penetrations (except for the amount of energy initially required in the case of reactions with negative Q values between ground states). The different curves shown in Figs. 7 and 8 correspond to the probabilities given by Eq. (10) normalized to the experimental data. This normalization includes spectroscopic information as well as Q-value-dependent correction factors. The solid lines correspond to the case of single-nucleon transfers or to the transfer of a cluster in the case of complex particles. The dashed and dotted lines correspond to different sequential transfers as indicated by the labels on the figures. These sequential transfer probabilities were calculated as the (uncorrelated) product of the probabilities for the individual steps. In each step the cores, transferred particle, and energy levels were appropriately taken following the above-described procedure for the single-nucleon or cluster case. The absolute normalization was fit to the short-distance region where the probabilities reach an approximately constant value. For the case of four-particle transfer, Fig. 8 also shows a band for each sequential transfer. Each band illustrates the effect produced by considering different sequences in the occurrence of transfer and excitation at every step, keeping the final excitation energy fixed in accordance with the experimental average Q value. In the calculations of the bands, the following cases were considered: (a) The excitation occurs after the exit-channel partition has been reached, (b) the excitation occurs in the entrance-channel partition, i.e., before any particle is transferred, and (c) the final excitation energy is shared among the different steps.

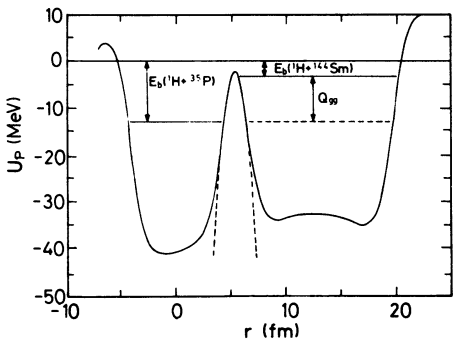

FIG. 9. Potential used in the calculation of the transmission probabilities of one-proton stripping in $^{36}S + ^{144}Sm$ at an internuclear distance of 13 fm.

The main feature observed in comparing the different calculations to the data refers to the distance at which "saturation" of the probabilities is reached. In general, the calculation predicts that when multinucleon transfer occurs in one step, the plateau extends to larger distances than when two or more steps are involved. As pointed out earlier, it becomes important to evaluate the sensitivity of this behavior with respect to the assumptions made in the calculation of the potential for complex fragments, in particular Eq. (13). For that purpose we may compare the value calculated using Eq. (13) for a two-proton cluster in ^{144}Sm, $V_{2p}^0 = 111.2$ MeV, to the value $V_{2p}^0 = 101$ MeV obtained by Künkel *et al.* [12] from fits to the experimental binding energies. If one considers, for example, the direct transfer of two protons from ^{36}S to ^{144}Sm, an uncertainty of about 10 MeV in V_{2p}^0 translates into a shift of about 0.02 fm in the reduced distance at which saturation occurs.

It is also apparent from Fig. 8 that the several possible ways of considering the excitation energy do not alter significantly the above-discussed behavior of the curves as a function of the number of steps involved, since there is little overlap between adjacent bands.

The comparison of the calculation with the data for multinucleon transfer shows, in general, a better agreement with processes that involve two or more steps rather than a single cluster transfer. The transfer of two pro-

tons in $^{36}S+^{154}Sm$ is somewhat unique in that there is no clear distinction between the calculated curves for sequential and direct transfers, whereas the data in this case extend to larger internuclear distances than both theoretical predictions.

B. Effects of nuclear deformation

The choice of a spherical projectile and the well-known structural characteristics of the samarium isotopes allow one to study the effect of nuclear deformation. Previous measurements of charged-particle transfer probabilities at large internuclear distances for oxygen-induced reactions on both ^{144}Sm and ^{154}Sm have shown noticeable differences between these two isotopes, which have been attributed to the corresponding different values of the quadrupole deformation parameter [4]. In a recent paper, Landowne and Dasso [5] have proposed a semiclassical model to explain this effect, from which a simple expression for the enhancement factor of the transfer cross sections at sufficiently low bombarding energies can be derived.

In order to address the question of the nuclear deformation in connection with the present data, we proceeded as follows. From the experimental mass-integrated angular distributions, we calculated transfer probabilities for ejectiles with $Z=14$ and 15, following the procedure of Sec. IV A. The usual apsidal distance D derived under the assumption of Coulomb trajectories [Eq. (2)] was replaced by the distance d between effective nuclear surfaces relevant to the occurrence of transfer:

$$d=D-\rho\ , \tag{14}$$

where ρ was taken as the internuclear distance corresponding to the experimental maximum of the angular distribution at 155 MeV. The same value was adopted for the 142-MeV data. If one defines an effective nuclear radius parameter ρ_0 through the equation

$$\rho=\rho_0(A_p^{1/3}+A_t^{1/3})\ , \tag{15}$$

the above-described procedure yields for ρ_0 a value around 1.52 ± 0.01 fm in all cases.

Figure 10 compares the transfer probabilities between ^{144}Sm and ^{154}Sm for projectilelike particles with $Z=14$ and 15 at both bombarding energies. One observes that the probabilities for ^{154}Sm are in all cases larger than those for ^{144}Sm. Also, there is a systematic difference between the two targets in the decay rates of these probabilities as a function of d, which suggests an enhancement of subbarrier transfer with increasing distance for ^{154}Sm. A similar behavior was observed in charged-particle transfer in $^{16}O+^{144,145}Sm$ [4], indicating that mass asymmetry does not play a significant role in the enhancement of the transfer. Table II summarizes the decay constants α associated with the solid curves of Fig. 10, which are least-squares fits of exponential shapes [Eq. (3)] to the data points.

In Ref. [5] the authors predicted an enhancement of 4.6 in transfer cross sections at low bombarding energies for spherical-on-deformed samarium systems considering a deformation parameter $\beta_2=0.29$ for ^{154}Sm. Table II shows the enhancement factors $\epsilon_{tr}=\sigma_{tr}^{154}/\sigma_{tr}^{144}$. In order

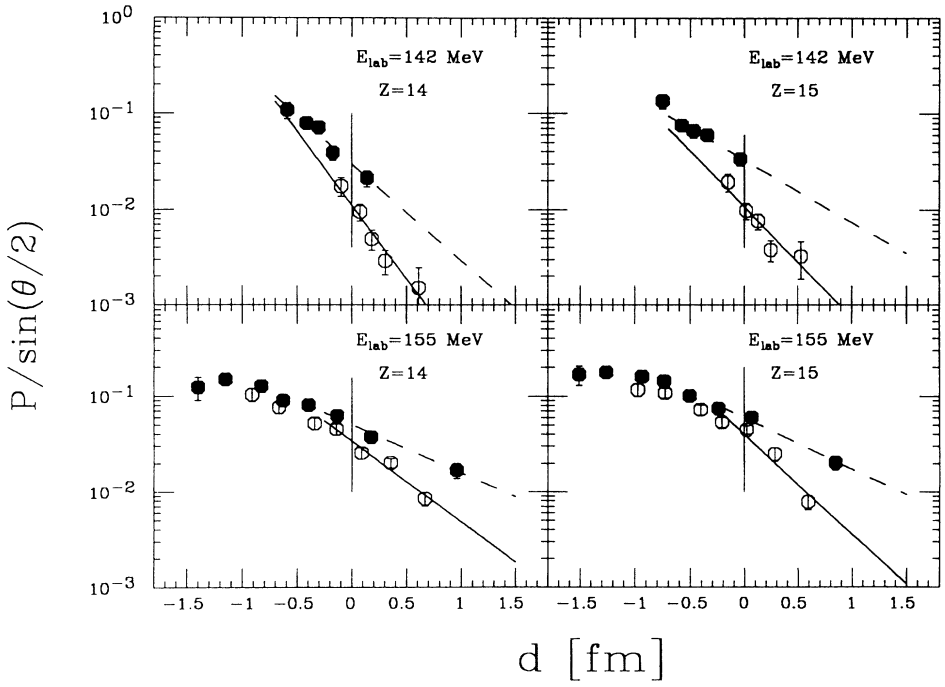

FIG. 10. Transfer probabilities in reactions leading to $Z=14$ and 15 ejectiles as a function of the distance between effective nuclear surfaces for the transfer process. Open symbols correspond to the ^{144}Sm target and solid symbols to ^{154}Sm.

TABLE II. Decay constant and deformed-to-spherical cross-section ratios.

E_{lab} (MeV)	Z	Target	α (fm^{-1})	ϵ_{tr}	ϵ_{DC}
142	14	^{144}Sm	3.55±0.1	6.9±2.0	6.4±1.0
		^{154}Sm	2.32±0.18		
	15	^{144}Sm	2.67±0.3	9.0±3.0	12.3±4.0
		^{154}Sm	1.50±0.2		
155	14	^{144}Sm	1.95±0.19	2.3±0.3	2.2±0.1
		^{154}Sm	1.16±0.19		
	15	^{144}Sm	2.41±0.27	2.4±3.0	2.7±0.4
		^{154}Sm	1.23±0.2		

to compare under more adequate conditions from the standpoint of the model, transfer cross sections for distant collisions, σ_{DC}, were obtained by integrating the differential cross sections over the forward-angle range starting from the angle corresponding to $d=0$. Table II also shows the enhancement for distant collisions, $\epsilon_{DC}=\sigma_{DC}^{154}/\sigma_{DC}^{144}$.

The analysis of the deformed-to-spherical ratios displayed in Table II indicates that there are significant enhancements in all cases. Also, the enhancement factors are not affected (within errors) when peripheral collisions (i.e., $d>0$) are selected, possibly with the exception of $Z=15$ at 142 MeV. On the other hand, there is an important dependence upon bombarding energy; the factor calculated in Ref. [5] is larger than the experimental values at 155 MeV, but it is smaller than those measured at 142 MeV.

C. Q-value dependence of stripping and pickup reactions

As mentioned above, the ^{36}S+^{144}Sm system presents charged-particle stripping as well as charged-particle pickup. This fact distinguishes this system from those with ^{16}O and ^{32}S as projectiles [4,13] where only stripping channels are open. In this particular system the transfer flow tends to lead the neutron-rich ^{36}S toward larger values in Z, whereas at the same time, from the ^{144}Sm point of view, a preferential formation of elements with lower values of Z is observed.

The nature of the different channels opened in these reactions can be understood from simple Q-value considerations. According to Eq. (5), for the ^{36}S+^{A}Sm systems, stripping reactions will have a Q distribution centered at negative Q values, whereas the Q distribution corresponding to pickup reactions will be centered at positive Q values. The width of these distributions is not well established since it depends, among other things, on the mechanism of the transfer process [14]. The Q_{opt} values for the pickup channels are 5.63 MeV (5.70 MeV) and 11.0 MeV (11.14 MeV) for the $+1p$ and $+2p$ transfers for ^{144}Sm (^{154}Sm) at $E_{lab}=155$ MeV. Therefore, since the two pickup channels in the ^{36}S+^{144}Sm reaction leading to Cl and Ar have positive Q values between ground states ($Q_{gg}=2.1$ and 8.0 MeV for $+1p$ and $+2p$, respectively), these transfer reactions are possible. In the ^{36}S+^{154}Sm case, on the other hand, very few pickup events were observed, which is to be expected from the larger energy difference between the Q_{opt} and Q_{gg} for these processes ($Q_{gg}=-0.6$ MeV for $1p$ pickup and $Q_{gg}=2.3$ MeV for $2p$ pickup).

The global trend of the cross sections can be visualized with the help of a driving potential defined as the difference between the ground-state Q values and Coulomb, rotational, and nuclear potential in the initial and final channels [15]. The transfer process can be characterized as a two-dimensional random walk on the N-Z plane led by the driving potential while an energy-conservation check is performed in each step. In this picture the driving potential determines the direction of the mass and charge flows, favoring the transfer steps leading to minima in the N-Z plane.

Calculations succeed in reproducing the experimental cross sections for charged-particle transfers in ^{36}S+^{144}Sm and ^{36}S+^{154}Sm systems at $E_{lab}=155$ MeV (see Fig. 11).

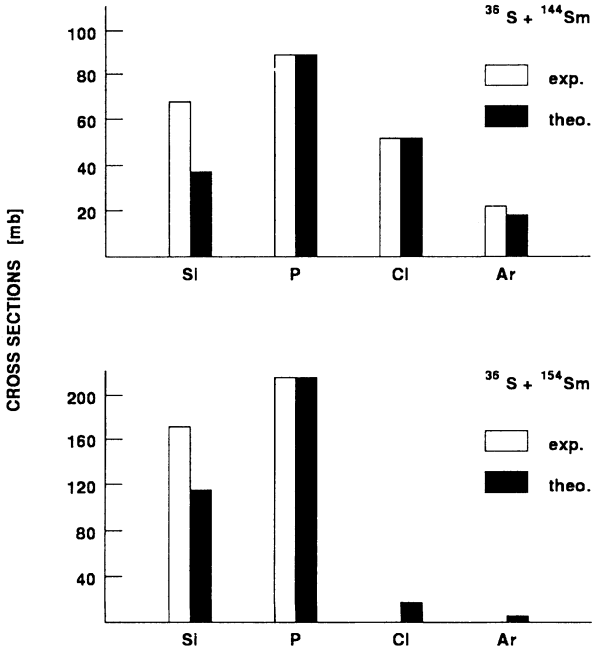

FIG. 11. Comparison of experimental cross sections and theoretical predictions obtained with a driving potential for the ^{36}S+^{144,154}Sm systems at $E_{lab}=155$ MeV. The calculations are normalized to the cross sections for $Z=15$.

For ^{154}Sm, only stripping reactions are expected. In the case of the $^{36}S+^{144}Sm$ system, the calculations predict stripping as well as pickup reactions as is experimentally observed. In these calculations best fits were achieved using a radius parameter for the Coulomb potential of $r_0=1.2$ fm for ^{144}Sm and $r_0=1.3$ fm for ^{154}Sm. Analogous calculations for the $^{32}S+^{144,154}Sm$ systems using these values of the radius also succeed in reproducing quantitatively the experimental data [13].

V. SUMMARY

Transfer reactions in the $^{36}S+^{144,154}Sm$ systems were measured at incident energies close to the Coulomb barrier with mass and charge identification. The transfer cross sections show increasing enhancements with increasing target deformation as pointed out in previous work with ^{16}O. The experimental enhancement factors are consistent with those obtained from a simple model that includes an angle-dependent separation between the nuclear surfaces in the transfer form factors. A simple semiclassical analysis considering direct and sequential tunneling between the interacting ions favors the second mechanism. The trend of the transfer flow can be understood with Q-value considerations; more quantitative results can be obtained in the framework of a driving-potential formalism.

ACKNOWLEDGMENTS

We want to thank Dr. K. E. Rehm for calculations using the driving potential and the tandem staff of Legnaro for their professional operation of the accelerator. We are also grateful to G. Monente for the careful preparation of large-area carbon foils and to A. Dal Bello for skillful technical assistance. Two of us (J.F.N. and J.T.) acknowledge the hospitality of Laboratori Nazionali di Legnaro during the experiment. This work was supported in part by the Consejo Nacional de Investigaciones Científicas y Tecnicas, CONICET, Argentina and by Grant No. 06 LM 171 of the Bundesministerium für Forschung und Technologie, Germany.

[1] M. Beckerman, Rep. Prog. Phys. **51**, 1047 (1988).
[2] C. H. Dasso, S. Landowne, and A. Winther, Nucl. Phys. **A405**, 381 (1983).
[3] R. Broglia, C. H. Dasso, S. Landowne, and A. Winther, Phys. Rev. C **27**, 2433 (1983).
[4] A. J. Pacheco, A. O. Macchiavelli, D. Abriola, D. E. DiGregorio, A. Etchegoyen, M. C. Etchegoyen, J. O. Fernández Niello, A. M. J. Ferrero, S. Gil, J. A. Kittl, and J. Testoni, Z. Phys. A **331**, 451 (1988).
[5] S. Landowne and C. H. Dasso, Phys. Lett B **202**, 31 (1988).
[6] R. Bass, *Nuclear Reactions with Heavy Ions* (Springer-Verlag, Berlin, 1980).
[7] K. Rudolph, D. Evers, P. Konrad, K.E.G. Löbner, U. Quade, S. J. Skorka, and I. Weidl, Nucl. Instrum. Methods **204**, 407 (1983).
[8] H. J. Kim, J. Gomez del Campo, D. Shapira, P. H. Stelson, and D. R. Napoli, Phys. Rev. C **43**, 1321 (1991).
[9] K. E. Rehm, in *Proceedings of the XII Workshop on Nuclear Physics,* Iguazu Falls, Argentina, 1989, edited by M. C. Cambiaggio *et al.* (World Scientific, Singapore, 1990), p. 212.
[10] U. Brosa and D.H.E. Gross, Z. Phys. A **298**, 91 (1980).
[11] D. L. Hill and J. A. Wheeler, Phys. Rev. **89**, 1102 (1953).
[12] R. Künkel, W. von Oertzen, H. Bohlen, B. Gebauer, H. A. Bosser, B. Kohlmeyer, J. Speer, F. Pühlhofer, and D. Schüll, Z. Phys. A **336**, 71 (1990).
[13] M. di Tada (private communication).
[14] L. Corradi, S. J. Skorka, U. Lenz, K.E.G. Löbner, P. R. Pascholati, U. Quade, K. Rudolph, W. Schomburg, M. Steinmayer, H. G. Thies, G. Montagnoli, D. R. Napoli, A. M. Stefanini, A. Tivelli, S. Beghini, F. Scarlassara, C. Signorini, and F. Soramel, Z. Phys. A **334**, 55 (1990).
[15] K. E. Rehm, A. M. van den Berg, J. J. Kolata, D. G. Kovar, W. Kutschera, G. Rosner, G.S.F. Stephans, and J. L. Yntema, Phys. Rev. C **37**, 2629 (1988).